



HAL
open science

Isotopically enriched polymorphs of dysprosium single molecule magnets

Y. Kishi, Fabrice Pointillart, B. Lefevre, F. Riobé, Boris Le Guennic, S. Golhen, O. Cador, O. Maury, H. Fujiwara, L. Ouahab

► **To cite this version:**

Y. Kishi, Fabrice Pointillart, B. Lefevre, F. Riobé, Boris Le Guennic, et al.. Isotopically enriched polymorphs of dysprosium single molecule magnets. *Chemical Communications*, 2017, 53 (25), pp.3575-3578. 10.1039/c7cc00317j . hal-01501267

HAL Id: hal-01501267

<https://univ-rennes.hal.science/hal-01501267v1>

Submitted on 6 Sep 2017

HAL is a multi-disciplinary open access archive for the deposit and dissemination of scientific research documents, whether they are published or not. The documents may come from teaching and research institutions in France or abroad, or from public or private research centers.

L'archive ouverte pluridisciplinaire **HAL**, est destinée au dépôt et à la diffusion de documents scientifiques de niveau recherche, publiés ou non, émanant des établissements d'enseignement et de recherche français ou étrangers, des laboratoires publics ou privés.

Isotopically Enriched Polymorphs of Dysprosium Single Molecule Magnets

Y. Kishi,^{a,b} F. Pointillart,^{*a} B. Lefevre,^a F. Riobé,^c B. Le Guennic,^a S. Golhen,^a O. Cador,^{*a} O. Maury,^c H. Fujiwara,^{*b} and L. Ouahab^a

The two triclinic Dy(t) and monoclinic Dy(m) polymorphs of [Dy(tta)₃(L)] with L=4-[6-(1,3-benzothiazol-2-yl)pyridin-3-yl]-4',5'-bis(methylthio)tetrathiafulvene behave as Single-Molecule Magnets with hysteresis loops open at zero-field. Magnetic properties were enhanced through magnetic dilution and ¹⁶⁴Dy isotopic enrichment which definitively support the importance of isotopes for the control of quantum magnets.

Single-Molecule Magnets (SMMs¹) fascinate chemists and physicists for more than two decades because they may offer the possibility to store magnetic information on a single molecule, *i.e.* one byte at the nanometer scale or less. Thus, they represent a promising alternative for high-density data storage, spintronics and quantum computing.² Exciting experimental results have been obtained recently on the basis of the quantum nature of molecular magnets.³ SMMs that are used in these studies mainly involve lanthanide ions because of their remarkable magnetic characteristics such as strong magnetic anisotropy and high magnetic moment. However the use of molecular magnets is currently locked by the too low temperatures at which the magnets operate. Two main reasons may be invoked: i) the height of the energy barrier which must be overcome to reverse the magnetic moment is too small and, consequently, the magnetic moment oscillates very rapidly between two opposite directions; ii) the magnetic moment can reverse very rapidly “through the barrier” by tunnelling effects. The magnetic bistability is generally lost at zero magnetic field leading to a butterfly shape hysteresis in case of Dy^{III}-based

mononuclear SMMs.⁴ Optimizations of the SMMs properties are thus required if applications are targeted. To do so, one first needs a perfect understanding of their magnetic properties. Recently, approaches using both *ab initio* calculations and the specific luminescence of lanthanides have been used to reach this required high-level of comprehension. The former permits to rationalize the experimental determination of the crystal field and the magnetic anisotropy axis orientation⁵ as well as to propose solutions to obtain high-temperature SMMs⁶ while the latter is used as a tool to probe the energy splitting of the M_J states of the multiplet ground state.⁷ To minimize fast zero-field tunnelling a strategy consists in reducing perturbations on the magnetic moment. In this context, some of us proposed to combine isotopic enrichment in free nuclear spin lanthanide⁸ and magnetic dilution.⁹ Moreover, the development of these SMMs involving donor-acceptor (D-A) type dyads based on tetrathiafulvalene (TTF) fragments¹⁰ could open the way to a new type of photo-conducting SMMs. For instance, the TTF-CH=CH-BZT (BZT=1,3-benzothiazole) ligand was synthesized to realize photo-switchable conductors and photoelectric conversion materials.¹¹ Recently, coordination complexes involving neutral and radical cation forms of this ligand were obtained by some of us.¹² In the present paper, the new 4-[6-(1,3-benzothiazol-2-yl)pyridin-3-yl]-4',5'-bis(methylthio)tetrathiafulvene ligand (L) (Scheme S1) was synthesized to be associated with the organometallic precursor Dy(tta)₃ to i) reproduce the coordination site already observed in [Dy(tta)(L¹)] (L¹=4,5-bis(propylthio)-tetrathiafulvalene-2-(2-pyridyl)benzimidazole-methyl-2-pyridine) (*i.e.* an N2O6 environment),^{4c,8} which leads to an electronic distribution imposing an axial ligand field and then a slow magnetic relaxation of the Dy magnetization, ii) control the dimensionality of the final product (*i.e.* discrete molecules) and ii) to involve the BZT moiety.

Polymorphism cannot be predicted but it has already demonstrated that it can highlight the crucial role of physical parameters such as intermolecular interactions.¹³ For the light lanthanide ions, the compounds crystallize in the P-1 triclinic

^a Institut des Sciences Chimiques de Rennes, UMR 6226 CNRS - Université de Rennes 1, 263 Avenue du Général Leclerc 35042 Rennes Cedex (France).

E-mail: fabrice.pointillart@univ-rennes1.fr, olivier.cador@univ-rennes1.fr

^b Department of Chemistry, Graduate School of Science, Osaka Prefecture University, 1-1 Gakuen-cho, Naka-ku, Sakai, Osaka, 599-8531, Japan.

hfuji@c.s.osakafu-u.ac.jp

^c Laboratoire de Chimie, UMR 5182 CNRS-ENS Lyon-Université Lyon 1, 46 Allée d'Italie, 69364 Lyon Cedex

^d † Electronic Supplementary Information (ESI) available: X-ray crystallographic files in CIF format, experimental and computational details, crystallographic data, and additional structural and magnetic figures and tables. See DOI: 10.1039/x0xx00000x

space group while for the heavy lanthanide ions, the compounds crystallize in the $P2_1/a$ monoclinic space group. Interestingly, $[Dy(tta)_3(L)]$ can crystallize in both forms, noted **Dy(t)** and **Dy(m)** for the triclinic and monoclinic space group, respectively (Table S1).

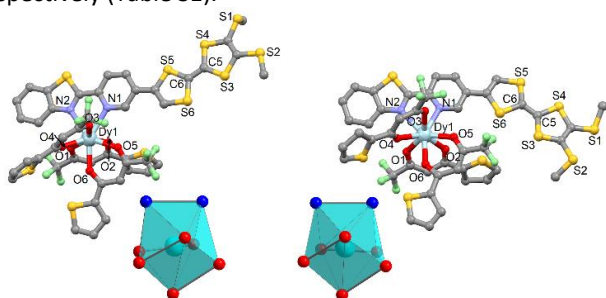


Fig. 1 Representation of the complex $[Dy(tta)_3L]$ in **Dy(t)** (left) and **Dy(m)** (right) with the coordination polyhedra in both structures (cyan, Dy; green, F; yellow, S; gray, C; blue, N; red, O). Thick lines on edges of polyhedra feature the atoms coming from the same bidentate ligand. Hydrogen atoms and CH_2Cl_2 molecule of crystallisation are omitted for clarity.

For both polymorphs, the $Dy(tta)_3$ metal-precursor is coordinated to the nitrogenated bischelating coordination site of the benzothiazole-2-pyridine moiety. The Dy^{III} ion is in a N_2O_6 square antiprism environment (D_{4d} symmetry) made of six oxygen and two nitrogen atoms that belong to three tta^- anions and one **L** ligand, respectively (Figs. 1 and S1). The respective ORTEP views for the complexes **Eu(t)** and **Y(m)** are depicted in Figs. S2-S3). The average Dy-N distances are similar in **Dy(t)** (2.583(5) Å) and **Dy(m)** (2.594(12) Å) (Table S2). The average Dy-O distances are comparable in **Dy(t)** (2.327(5) Å) and **Dy(m)** (2.326(9) Å) (Table S2). Nevertheless a deeper analysis revealed that the shortest Dy-O bond lengths involve O3 and O4 in **Dy(t)**, which are localised above the plan formed by the nitrogen atoms, while for **Dy(m)** the shortest Dy-O bond lengths involve O1 and O4 which are localised from either side of the plan formed by the nitrogen atoms. The latter observation is favourable to a better localisation of the most negative charges along an axis in **Dy(m)** than in **Dy(t)**. Two different conformations of **L** are present in **Dy(t)** and **Dy(m)**. **L** turns up in **Dy(t)** and down in **Dy(m)**. The polyhedron in **Dy(m)** is close to a square antiprism while in **Dy(t)** the polyhedron is halfway between a square antiprism and a triangular dodecahedron (Table S3). The up or down rotation of the ligand **L** depends on the size of the lanthanide ion, with the up rotation for large lanthanide ions (Eu^{III} for example) and the down rotation observed for small lanthanide ions (Y^{III} for example). In between, for Dy^{III} , the two isomers are obtained. The C=C central bond lengths of the TTF core attest of the neutrality of **L** in both polymorphs (C5=C6=1.349(9) Å and 1.350(20) Å in **Dy(t)** and **Dy(m)**, respectively). The crystal packing of **Dy(t)** shows several intermolecular interactions guarantying the cohesion of the crystal (Fig. S4) and the crystal packing of **Dy(m)** is sensibly different compared to the one of **Dy(t)** due to the rotation of **L** (Fig. S5). The intermolecular shortest Dy-Dy distances have been found equal to 8.978 Å and 9.620 Å for **Dy(t)** and **Dy(m)**, respectively. The electrochemical properties (Fig. S6, Table S4) attest the redox-activity of **L** in the complexes.

The room temperature values of $\chi_M T$ for both **Dy(t)** and **Dy(m)** (13.87 and 13.96 $cm^3 K mol^{-1}$ respectively) are close to

the expected 14.17 $cm^3 K mol^{-1}$ for a ${}^6H_{15/2}$ ground-state multiplet.¹⁴ On cooling, $\chi_M T$'s decrease monotonically down to 11.5 and 11.1 $cm^3 K mol^{-1}$ for **Dy(t)** and **Dy(m)**, respectively (Fig. S7). Both magnetization curves at 2 K are perfectly superimposed with saturation magnetization equal to 4.9 $N\beta$ (Fig. S8) in agreement with the stabilization of the Ising component ($M_J = \pm 15/2$) of ${}^6H_{15/2}$ in a N_2O_6 environment.⁴ **Erreur ! Signet non défini.** *Ab-initio* calculations performed on isolated molecules from single crystal X-ray structures (see Computational details) fairly reproduce the thermal behaviours of the magnetic susceptibilities as well as the field variation of the magnetizations at low temperature (Figs. S7 and S8). In the frame of the effective spin $1/2$ approximation, the principal Zeeman tensor values of the ground-state doublets are $\{g_x=0.001, g_y=0.002, g_z=19.558\}$ and $\{g_x=0.012, g_y=0.022, g_z=19.435\}$ for **Dy(t)** and **Dy(m)**, respectively. These values are very close to the $\{g_x=0.0, g_y=0.0, g_z=20\}$ expected for a pure $M_J = \pm 15/2$ Ising component. The ground-state wavefunctions corroborate these statements (Table S5). The angular dependences of the magnetization of an assembly of **Dy(t)** single crystals, preliminarily oriented by single crystal X-ray diffraction, have been measured in three perpendicular planes.¹⁵ The susceptibility tensor is extracted in fitting the data with the following equation (Fig. S9): $\chi_M T = M/H = \chi_{\alpha\alpha} T \cos^2 \theta + 2\chi_{\alpha\beta} T \sin \theta \cos \theta + \chi_{\beta\beta} T \sin^2 \theta$ where α and β are the directions X, Y and Z (Fig. S10) in a cyclic permutation and θ is the angle between the magnetic field H and α . In the effective spin $1/2$ formalism, the Zeeman principal values are $g_x=6.06, g_y=17.66$ and $g_z=4.37$ which clearly feature an axial behaviour of the magnetic moment. The orientation of the largest component of the Zeeman tensor is represented on Fig. 2a. As expected from previous studies on similar N_2O_6 coordination sphere⁴ the easy magnetic axis (g_z) is almost aligned with the most negatively charged direction of the N_2O_6 polyhedron (Fig 2a). The calculated g_z axis is in turn at 8.5° from the experimental one which corresponds to an excellent agreement (Fig. 2a). In **Dy(m)** the calculated magnetic axis has exactly the same orientation than in **Dy(t)** (Fig. S11). Both **Dy(t)** and **Dy(m)** behave as SMMs at low temperature in zero external dc field (0 Oe) with frequency dependence of the two components of the ac susceptibility (Figs. 2b and S12). Clearly, at the lowest temperatures (~ 2 K) the triclinic form relaxes slower than the monoclinic form. This might be due to stronger intermolecular interactions in **Dy(m)** than in **Dy(t)** despite the fact that the intermolecular Dy-Dy distances are equivalent in both forms. Indeed, intermolecular coupling of dipolar origin not only depends on distances but also on the orientations of the magnetic moments. For both compounds the characteristic relaxation times are extracted using an extended Debye model (Tables S6 and S7). For both materials the temperature dependence of the relaxation time can be fairly well reproduced with a combination of a thermally (Arrhenius) dependent and a thermally independent processes: $\tau^{-1} = \tau_0^{-1} \exp(-\Delta/kT) + \tau_{TI}^{-1}$ (where Δ is the energy barrier, τ_0 the intrinsic relaxation time and τ_{TI} the thermally independent relaxation time). The best-fitted curves are represented in Fig. 2c with the following parameters: $\tau_0 = 1.1(2) \times 10^{-5}$ s, $\Delta = 57(3)$ K and $\tau_{TI} = 4.6(2) \times 10^{-3}$ s for

Dy(t) and $\tau_0=1.0(1)\times 10^{-5}$ s, $\Delta=42(2)$ K and $\tau_{11}=1.9(1)\times 10^{-3}$ s for **Dy(m)**. The application of a moderate external field of 1 kOe dramatically slows down the relaxation process (Fig. S13). The relaxation times, extracted at higher temperatures than 4 K and under 1 kOe (Tables S8 and S9) follow an Arrhenius law (Fig. 2c) with the following parameters: $\tau_0=1.2(3)\times 10^{-6}$ s, $\Delta=96(4)$ K for **Dy(t)** and $\tau_0=2.7(4)\times 10^{-6}$ s, $\Delta=65(2)$ K for **Dy(m)**. Here again, **Dy(t)** relaxes slower than **Dy(m)**. This is supported by the calculated magnetization blocking barrier for both compounds (Fig. S14) that shows more efficient relaxation pathways for **Dy(m)** than **Dy(t)**. The barrier height in **Dy(m)** does not differ from the one observed in $[\text{Dy}(\text{tta})_3\text{L}^1]$ ($\text{L}^1=4,5\text{-bis}(\text{propylthio})\text{-tetrathiafulvalene-2-(2-pyridyl)benzimidazole-methyl-2-pyridine}$)^{4c} which is made of the same N_2O_6 coordination polyhedron.

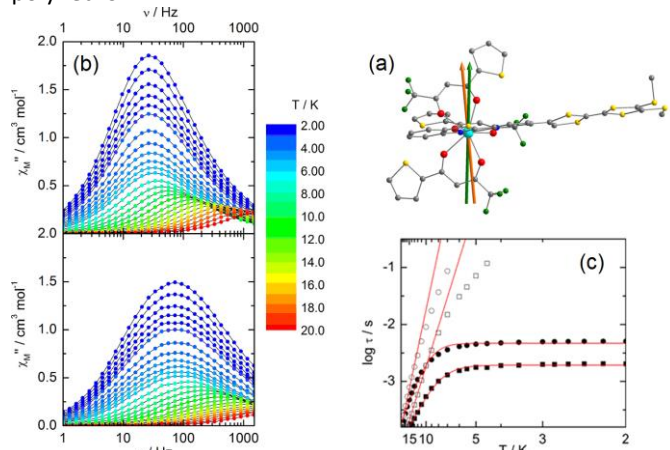


Fig. 2 (a) Structure of $[\text{Dy}(\text{tta})_3\text{L}]$ in **Dy(t)**. Experimental (dark green) and theoretical (orange) magnetic anisotropy axis. H atoms have been omitted for clarity in both representations. (b) (top) Frequency dependence of the out-of-phase component, χ''_M , of the ac susceptibility for **Dy(t)** (top) and **Dy(m)** (bottom). (c) Log scale plots of the temperature dependence of the relaxation time of the magnetic moment in **Dy(t)** (circles) and **Dy(m)** (squares) at zero external field (full symbols) and at 1 kOe (empty symbols). Red lines correspond to the best-fitted curves with Arrhenius or modified Arrhenius laws (see text).

The coordination is more distorted in **Dy(m)** than in $[\text{Dy}(\text{tta})_3\text{L}^1]$ ($\text{CShM}_{\text{SAPR-8}}=0.816$ vs. 0.537) and even more distorted ($\text{CShM}_{\text{SAPR-8}}=1.140$) in **Dy(t)** with however the highest barrier of the series. Then one must conclude that there is actually no clear correlation between the polyhedron distortion and the barrier height. The predominant parameter could be the electronic distribution of the first neighbouring atoms of the Dy^{III} which may be more favourable in **Dy(t)** than in **Dy(m)**. The calculated axial tensor (g_z) and the transversal components (g_x and g_y) are respectively higher and lower in **Dy(t)** than **Dy(m)** which is in agreement with i) the slower magnetic relaxation observed in **Dy(t)** compared to **Dy(m)** and ii) the difference of Dy-X bond lengths observed in the X-ray structures. The calculated energy gaps between the ground-state doublet and the first excited-state doublet are 181, 226 and 197 K for $[\text{Dy}(\text{tta})_3\text{L}^1]$, **Dy(t)** and **Dy(m)**, respectively. In these cases, the highest calculated gap coincides with the highest measured barrier. In order to improve the efficiency of our nanomagnets in zero field we have applied the same strategy that we have introduced in a recent work⁸ which is: 1) to dilute the magnet in an isomorphous diamagnetic matrix and 2) to substitute the natural dysprosium element by one of its isotope which does not carry nuclear spin (^{164}Dy). As expected, dc magnetic

measurements on $^{164}\text{Dy}(\text{m})$ perfectly superimpose with those of **Dy(m)** (Fig. S15). In contrast, ac magnetic measurements reveal differences. At 0 Oe, the relaxation time is slower in the thermally independent regime (Table S10) and identical in the thermally activated regime ($\tau_0=8.4(2)\times 10^{-6}$ s, $\Delta=41(2)$ K and $\tau_{11}=3.11(8)\times 10^{-3}$ s, Fig. S16). Under 1 kOe the temperature dependence of the relaxation time almost coincides with the natural product **Dy(m)** ($\tau_0=2.4(6)\times 10^{-6}$ s, $\Delta=60(2)$ K, Table S10 and Fig. S16). In the quantum regime the suppression of the nuclear magnetic moment increases the relaxation time by a factor of 2. The diamagnetic molecule $[\text{Y}(\text{tta})_3\text{L}]$ crystallizes in the monoclinic phase (**Y(m)**) (Table S1). Then it has been doped with Dy^{III} to form $\text{Dy}_{0.02}\text{Y}_{0.98}(\text{m})$. The main consequence of the dilution is the release of the quantum regime at 0 Oe (Table S12, Fig. S17). Indeed, at 4 K the relaxation time has been multiplied almost by 2000. It is also thermally dependent in the whole temperature range (Fig. S16) with dynamic parameters $\tau_0=4.5(7)\times 10^{-6}$ s and $\Delta=76(2)$ K. An external field of 1 kOe does not greatly modify the relaxation (Fig. S18) which is almost field independent down to 10 K ($\tau_0=2.9(7)\times 10^{-6}$ s, $\Delta=82(3)$ K, Table S13 and Fig. S16). At lower temperatures the 1 kOe relaxation becomes slower than at 0 Oe. The final stage is to dope **Y(m)** with $^{164}\text{Dy}^{\text{III}}$ isotope to form $^{164}\text{Dy}_{0.07}\text{Y}_{0.93}(\text{m})$ (Table S14). The thermal behaviour of the relaxation time of $^{164}\text{Dy}_{0.07}\text{Y}_{0.93}(\text{m})$ at 0 Oe (Fig. S18, Table S15) as well as at 1 kOe (Fig. S20, Table S16) follows the curves obtained for $\text{Dy}_{0.02}\text{Y}_{0.98}(\text{m})$ above 10 K. Dynamic parameters in the high temperature (above 10 K) can be reproduced with $\tau_0=3.2(6)\times 10^{-6}$ s and $\Delta=82(3)$ K at 0 Oe ($\tau_0=2.4(6)\times 10^{-6}$ s and $\Delta=84(4)$ K at 1kOe). These values are in good agreement with all previously fitted parameters. Since **Dy(t)** has better magnetic properties than **Dy(m)**, it was then logical to apply the same methodology (dilution+isotopic enrichment) to the triclinic form with the condition to find a diamagnetic isomorphous matrix crystallising in the triclinic system. The multiplet ground-state $^7\text{F}_0$ of Eu^{III} is non-magnetic and therefore should induce minimal magnetic perturbation at low temperature that might be neglected in the dilution experiments. At room temperature $\chi_{\text{M}}T$ of **Eu(t)** is equal to $1.37 \text{ cm}^3 \text{ K mol}^{-1}$ and decreases monotonically on cooling down to $0.03 \text{ cm}^3 \text{ K mol}^{-1}$ at 5 K.¹⁶ At 5 K, The magnetism from Eu^{III} in **Eu(t)** represents only 0.3% of the signal of **Dy(t)**. Therefore, we have prepared $^{164}\text{Dy}_{0.05}\text{Eu}_{0.95}(\text{t})$ (Fig. S22) in which the magnetism from Eu^{III} is estimated to represent only 5% of the magnetization at 5 K. At 0 Oe the curves for the three doped samples ($^{164}\text{Dy}_{0.05}\text{Eu}_{0.95}(\text{t})$) (Figs S16 and S23, Table S17), $^{164}\text{Dy}_{0.07}\text{Y}_{0.93}(\text{m})$ and $\text{Dy}_{0.02}\text{Y}_{0.98}(\text{m})$ almost collapse on the same master curve at higher temperature than 3 K ($\tau_0=4.4(9)\times 10^{-6}$ s and $\Delta=74(3)$ K for $^{164}\text{Dy}_{0.05}\text{Eu}_{0.95}(\text{t})$). At 1 kOe all the curves perfectly superimpose above 5 K ($\tau_0=3.3(7)\times 10^{-6}$ s and $\Delta=80(3)$ K for $^{164}\text{Dy}_{0.05}\text{Eu}_{0.95}(\text{t})$, Figs. S16 and S24, Table S18). All the extracted dynamic parameters are collected in Table S19.

Butterfly type hysteresis loops are observed for **Dy(m)** and **Dy(t)** at lower temperature than 3 K (Figs. 3a and S25). They close at the origin because of the fast zero-field relaxation. Whatever the temperature the loop is broader for **Dy(t)** than for **Dy(m)** which reflects the slower relaxation in **Dy(t)**. For both yttrium-based doped samples $\text{Dy}_{0.02}\text{Y}_{0.98}(\text{m})$ and

$^{164}\text{Dy}_{0.07}\text{Y}_{0.93}(\text{m})$ the hysteresis loops open also in field below 3.5 K (Figs. 3b and S26) at slightly higher temperature than $\text{Dy}(\text{t})$ and $\text{Dy}(\text{m})$. However, the minimization of the internal field also opens the loops at zero field.

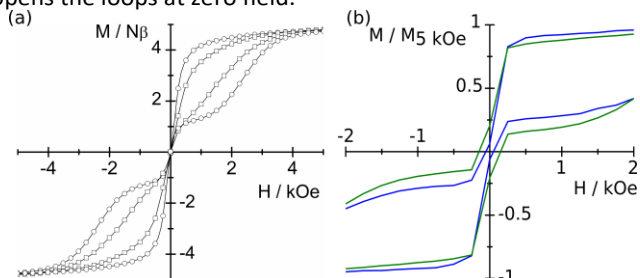


Fig. 3 (a) Hysteresis loops for (a) $\text{Dy}(\text{t})$ (circles) and $\text{Dy}(\text{m})$ (squares) for (b) $^{164}\text{Dy}_{0.07}\text{Y}_{0.93}(\text{m})$ (olive) and $\text{Dy}_{0.02}\text{Y}_{0.98}(\text{m})$ (blue) recorded at 500 mK at 16 Oe s^{-1} .

At ^3He temperature (500 mK) the isotopically enriched material $^{164}\text{Dy}_{0.07}\text{Y}_{0.93}(\text{m})$ is the best magnet (Fig. 3b), as expected. The remnant magnetization is multiplied by a factor of three with the isotopic enrichment. Finally, $^{164}\text{Dy}_{0.05}\text{Eu}_{0.95}(\text{t})$ displays similar hysteresis (Fig. S27) than $^{164}\text{Dy}_{0.07}\text{Y}_{0.93}(\text{m})$ which opens below 3.5 K. There is no striking difference between the hysteresis loops of these two compounds whatever the temperature (Fig. S28). The differences observed in condensed pure crystalline phase are not valid anymore once the molecule is dispersed in a crystalline diamagnetic medium. This confirms that a large part of the relaxation of the molecular magnetic moment at extremely low temperature is governed by the coupling with the surrounding moments.

In conclusion, a series of mononuclear coordination complexes of formula $[\text{Ln}(\text{tta})_3(\text{L})] \cdot x\text{CH}_2\text{Cl}_2$ ($x=0$ or 1) highlights two polymorphs depending of the lanthanide radii. The two Dy^{III} polymorphs behave as SMMs with an opened hysteresis loop at low temperature. Such magnetic bistability can be generally attributed to the combination of the N_2O_6 environment with $\text{Dy}(\text{tta})_3$ unit. The triclinic form presents a slower magnetic relaxation than its monoclinic analogue. Unambiguously, the symmetry of the coordination polyhedron plays a major role to determine the energy splitting diagram of the ground state multiplet. However, the electronic distribution at the surface of the coordination sphere of the lanthanide is at least as important as symmetry considerations. Finally the magnetic properties have been enhanced using magnetic dilution and isotopic enrichment in nuclear spin free Dysprosium which support the importance of isotopes for the control of quantum magnets.

This work was supported by Région Bretagne, Rennes Métropole, CNRS, Université de Rennes 1, FEDER and the ANR (ANR-13-BS07-0022-01) for financial support. B.L.G. thanks the French GENCI/IDRIS-CINES centres for high-performance computing resources. The authors thank Miss Chika Hashimoto for the synthesis of **L** ligand.

Notes and references

1 R. Sessoli, H. L. Tsai, A. R. Schake, S. Y. Wang, J. B. Vincent, K. Folting, D. Gatteschi, G. Christou, D. N. Hendrickson, *J. Am. Chem. Soc.* 1993, **115**, 1804.

2 (a) C. J. Wedge, G. A. Timco, E. T. Spielberg, R. E. George, F. Tuna, S. Rigby, E. J. L. McInnes, R. E. P. Winpenny, S. J. Blundell, A. Ardavan, *Phys. Rev. Lett.* 2012, **108**, 107204. (b) N. Papisimakis, S. Thongrattanasiri, N. I. Zheludev, F. J. Garcia de Abajo, *Light: Sci. Appl.* 2013, **2**, e78. (c) S. Sanvito, *Chem. Soc. Rev.* 2011, **40**, 3336. (d) M. Mannini, F. Pineider, P. Saintavit, C. Danieli, E. Otero, C. Sciancalepore, A. M. Talarico, M.-A. Arrio, A. Cornia, D. Gatteschi, R. Sessoli, *Nat. Mater.* 2009, **8**, 194. (e) L. Tesi, E. Lucaccini, I. Cimatti, M. Perfetti, M. Mannini, M. Atzori, E. Morra, M. Chiesa, A. Caneschi, L. Sorace, R. Sessoli, *Chem. Sci.* 2016, **7**, 2074; (f) K. S. Pedersen, A.-M. Ariciu, S. McAdams, H. Weihe, J. Bendix, F. Tuna, S. Piligkos, *J. Am. Chem. Soc.* 2016, **138**, 5801.

3 S. Thiele, F. Balestro, R. Ballou, S. Klyatskaya, M. Ruben, W. Wernsdorfer, *Science* 2014, **344**, 1135.

4 (a) P. Zhang, L. Zhang, C. Wang, S. Xue, S.-Y. Lin, J. Tang, *J. Am. Chem. Soc.* 2014, **136**, 4484. (b) Y. Bi, Y.-N. Guo, L. Zhao, Y. Guo, S.-Y. Lin, S.-D. Jiang, J. Tang, B.-W. Wang, S. Gao, *Chem. Eur. J.* 2011, **17**, 12476. (c) F. Tuna, C. A. Smith, M. Bodensteiner, L. Ungur, L. Chibotaru, E. J. L. McInnes, R. E. P. Winpenny, D. Collison, R. A. Layfield, *Angew. Chem. Int. Ed.* 2012, **51**, 6976. (d) T. T. da Cunha, J. Jung, M.-E. Boulon, G. Campo, F. Pointillart, C. L. M. Pereira, B. Le Guennic, O. Cador, K. Bernot, F. Pineider, S. Golhen, L. Ouahab, *J. Am. Chem. Soc.* 2013, **135**, 16332. (e) Y.-N. Huo, L. Ungur, G. E. Granroth, A. K. Powell, C. Wu, S. E. Nagler, J. Tang, L. F. Chibotaru, D. Cui, *Sci. Rep.* 2014, **4**, 5471. (f) J. Wu, J. Jung, P. Zhang, H. Zhang, J. Tang, B. Le Guennic, *Chem. Sci.* 2016, **7**, 3632.

5 (a) L. Ungur, S.-Y. Lin, J. Tang, L. F. Chibotaru, *Chem. Soc. Rev.* 2014, **43**, 6894 and references therein. (b) F. Pointillart, J. Jung, R. Berraud-Pache, B. Le Guennic, V. Dorcet, S. Golhen, O. Cador, O. Maury, Y. Guyot, S. Decurtins, S.-X. Liu, L. Ouahab, *Inorg. Chem.* 2015, **54**, 5384. (c) C. Y. Chow, H. Bolvin, V. E. Campbell, R. Guillot, J. F. Kampf, W. Wernsdorfer, F. V. Gendron, J. Autschbach, V. L. Pecoraro, T. Mallah, *Chem. Sci.* 2015, **6**, 4148.

6 N. F. Chilton, C. A. P. Goodwin, D. P. Mills, R. E. P. Winpenny, *Chem. Commun.* 2015, **51**, 101.

7 (a) F. Pointillart, B. Le Guennic, S. Golhen, O. Cador, O. Maury, L. Ouahab, *Chem. Commun.* 2013, **49**, 615. (b) J. Long, R. Vallat, R. A. S. Ferreira, L. D. Carlos, F. A. A. Paz, Y. Guari, J. Larionova, *Chem. Commun.* 2012, **48**, 9974. (c) M. Ren, S.-S. Bao, R. A. S. Ferreira, L.-M. Zheng, L. D. Carlos, *Chem. Commun.* 2014, **50**, 7621.

8 F. Pointillart, K. Bernot, S. Golhen, B. Le Guennic, T. Guizouarn, L. Ouahab, O. Cador, *Angew. Chem. Int. Ed.* 2015, **54**, 1504.

9 (a) S.-D. Jiang, B.-W. Wang, G. Su, Z.-M. Wang, S. Gao, *Angew. Chem. Int. Ed.* 2010, **49**, 7448; *Angew. Chem.* 2010, **122**, 7610. (b) F. Habib, P.-H. Lin, J. Long, I. Korobkov, W. Wernsdorfer, M. Murugesu, *J. Am. Chem. Soc.* 2011, **133**, 8830.

10 (a) K. Soussi, J. Jung, F. Pointillart, B. Le Guennic, B. Lefevre, S. Golhen, O. Cador, Y. Guyot, O. Maury, L. Ouahab *Inorg. Chem. Front.* 2015, **2**, 1105. (b) F. Pointillart, B. Le Guennic, O. Cador, O. Maury, L. Ouahab, *Acc. Chem. Res.* 2015, **48**, 2834.

11 H. Fujiwara, S. Yokota, S. Hayashi, S. Takemoto, H. Matsuzaka, *Physica B* 2010, **405**, S15.

12 S. Yokota, K. Tsujimoto, S. Hayashi, F. Pointillart, L. Ouahab, H. Fujiwara, *Inorg. Chem.* 2013, **52**, 6543.

13 F. Pointillart, K. Bernot, G. Poneti, R. Sessoli, *Inorg. Chem.* 2012, **51**, 12218.

14 O. Kahn, *Molecular Magnetism*, VCH: Weinheim, 1993.

15 J. Jung, O. Cador, K. Bernot, F. Pointillart, J. Luzon, B. Le Guennic, *Beilstein J. Nanotechnol.* 2014, **5**, 2267.

16 G. Lapadula, A. Bourdolle, F. Allouche, M. Cpnley, I. Del Rosa, L. Maron, W. W. Lukens, Y. Guyot, C. Andraud, S. Brasselet, C. Copéret, O. Maury, R. A. Andersen, *Chem. Mater.* 2014, **26**, 1062.